energy&fuels

pubs.acs.org/EF Article

Dynamic Fluid Interactions during CO_2-Enhanced Coalbed Methane and CO_2 Sequestration in Coal Seams. Part 1: CO_2−CH_4 Interactions

Sijian Zheng, Yanbin Yao,* Derek Elsworth, Dameng Liu, and Yidong Cai

Cite This: *Energy Fuels* 2020, 34, 8274−8282 Read Online

ACCESS | Metrics & More | Article Recommendations

ABSTRACT: The injection of CO_2 into coalbed methane (CBM) reservoirs to enhance methane recovery has a second desirable benefit in simultaneously sequestering CO_2. However, the real-time dynamic evolution of native adsorbed and rejected non-adsorbed methane during the process of CO_2-enhanced coalbed methane (CO_2-ECBM) production remains poorly constrained as a result of the nonlinear and hysteretic response of both CO_2−CH_4 interactions (part 1) and CO_2−H_2O wettability (part 2) of the coal under recreated reservoir conditions. In part 1, we apply calibrated nuclear magnetic resonance (NMR) to explore mechanisms of methane desorption and CO_2 replacement during multiple cycles of CO_2-ECBM flooding under recreated *in situ* conditions. Results for contrasting sub-bituminous coal and anthracite indicate that the adsorbed methane sweep efficiency is improved by ∼16−26% with a single injection of CO_2 over mere *in situ* desorption. Furthermore, CO_2−CH_4 displacement rates evolve during each CO_2 injection cycle, first declining rapidly and then stabilizing with a long desorptive tail. Importantly, the cumulative methane sweep efficiency increases monotonically with successive cycles of CO_2 injection, albeit at a reducing incremental efficiency, identifying the utility of cyclic CO_2-ECBM as an effective method in both CO_2 sequestration and enhanced gas recovery. Observed ratios of CO_2 sorption capacities to CH_4 recovery are 5.0 and 2.2 for sub-bituminous coal and anthracite, respectively, demonstrating an elevated potential for CO_2 sequestration in sub-bituminous coals and more favorable CO_2-ECBM recovery in anthracite, per unit mass of CO_2 injected.

1. INTRODUCTION

Carbon dioxide (CO_2) is a potent greenhouse gas, with the excess CO_2 emission posing a threat to human survival and the earthly environment.[1,2] According to the latest report of the Global Carbon Project, the total global CO_2 emissions reached ∼37 billion tons; the excessive emission of it could result in serious problems in global warming and sea levels rising.[3] Various methods have been applied to reduce the excessive emissions of CO_2 in the atmosphere, including geological sequestration in depleted hydrocarbon reservoirs, deep coal seams, and salt caverns.[4]

Recovery of coalbed methane (CBM) contributes an essential role in some counties (e.g., Australia, Canada, and China) in providing clean energy and reducing greenhouse gas emissions over burning coal.[5−11] Conventional methods of recovery are by reservoir depressurization, to recover adsorbed methane.[12,13] However, the resulting methane recovery is commonly less than 50% of the original gas in place as a result of the limiting characteristics of the reservoir (e.g., permeability and pore size distribution), leaving adsorbed methane in place.[14,15] Typically, greater than 95% of methane in coals exists in the adsorbed state,[16−18] requiring efficient methods to recover residual adsorbed methane. Injection of CO_2-enhanced coalbed methane (CO_2-ECBM) recovery from reservoirs is an effective method to combine methane recovery with the benefit of CO_2 geological sequestration and storage[19−23] as a result of the higher adsorption capacity to coal than methane, which may be used to displace adsorbed methane and store CO_2.[24−27]

In field application, from 1995 to 2001, 336 000 tons of CO_2 was injected into four wells in the San Juan Basin, U.S.A., with methane recovery improved from 77 to 95% following CO_2 injection.[28] Moreover, in April 2010, 233.6 tons of CO_2 was injected into well SX-001 in the Qinshui Basin over a 2 month period, resulting in a 2.5-fold increase in the post-injection methane production rate.[29] Experimental observations reveal that the sorption capacity of CO_2 is ∼2−10 times than that of methane in coals, enabling elevated methane recovery by CO_2-ECBM.[30−33] In comparison to natural desorption, methane desorption could be improved by 9−57% using CO_2 on coals.[34] Typically, during the process of CO_2-ECBM, CO_2 injection pressure is a critical parameter defining improvement in methane recovery; higher injection pressures drive higher methane sweep efficiency.[12] However, the improvement in the methane recovery rate reduces with an increase in CO_2 injection pressure.[26] CO_2/CH_4 exchange de/sorption experiments suggest that methane is entirely displaced after injecting double the mass of CO_2 relative to previously adsorbed methane, at least for briquette coals and also apparent in intact coals.[15,35,36] Laboratory experiments have demonstrated that a

Received: April 29, 2020
Revised: June 12, 2020
Published: June 15, 2020

https://dx.doi.org/10.1021/acs.energyfuels.0c01371
Energy Fuels 2020, 34, 8274−8282

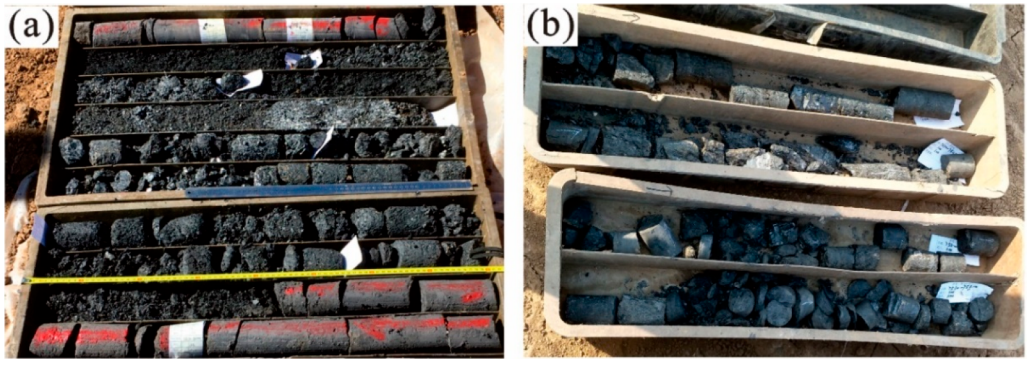

Figure 1. Deep-well core samples used in this study (a, sub-bituminous coal; b, anthracite).

Table 1. Basic Petrophysical Characteristics of the Selected Coal Samples[a]

						maceral composition (%)			
sample	coal basin	$R_{o,m}$ (%)	depth (m)	P_{in} (MPa)	P_{ab} (MPa)	V	I	E	M
sub-bituminous	southern Junggar	0.54	712	4.2	1.1	76.5	21.7	1.1	0.7
anthracite	southern Qinshui	3.16	557	3.5	0.9	87.9	9.2	2.1	0.8

[a] $R_{o,m}$, maximum vitrinite reflectance; P_{in}, *in situ* reservoir pressure; P_{ab}, abandonment pressure; V, vitrinite; I, inertinite; E, exinite; and M, minerals.

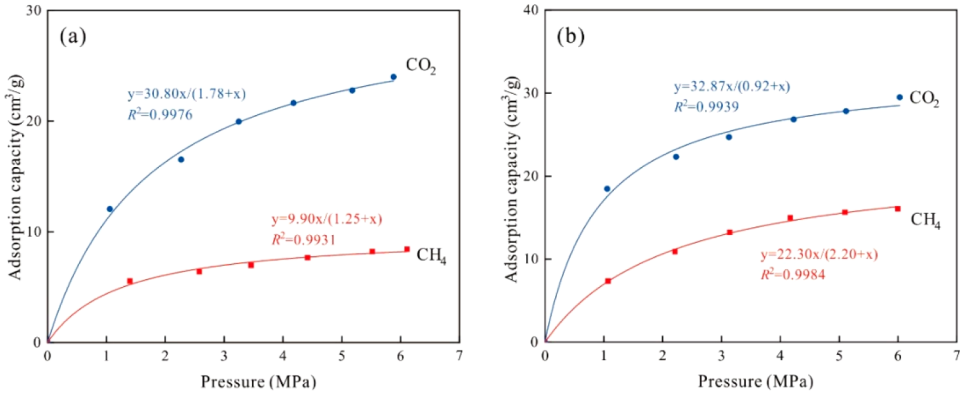

Figure 2. CO_2 and methane adsorption isotherms determined by the volumetric adsorption method (a, sub-bituminous coal; b, anthracite).

single large mass of CO_2 rapidly injected to steam could accelerate reservoir pressure buildup[37,38] but results in a dramatic decrease in the capacity of CO_2 and consequent decrease in CBM production.[26,37] Conversely, multiple cycles of CO_2 injection to coals may enhance the internal pore connectivity and increase methane sweep efficiency.[37] However, few studies have investigated the real-time dynamic de/sorption of CH_4/CO_2 over multiple cycles, which is the focus of this work.

The nuclear magnetic resonance (NMR) method is widely used to evaluate the petrophysical properties of hydrogen-bearing reservoir fluids (i.e., water and methane), including evolutions of pore size distributions, permeability, and methane adsorption characteristics.[39−45] NMR has been demonstrated as an accurate method to probe methane de/sorption capacity, including with water[46] and CO_2.[47] This latter study was only to 4 MPa and for a single injection rather than multiple cycles of CO_2 injection. Additionally, it is worth noticing that the application of NMR to reveal the characterization of multiple cycles of injection of the CO_2-ECBM process under *in situ* conditions is relatively uncharted. In multiple spaces of the CBM reservoirs, the characterization of multiphase fluid interactions during CO_2-ECBM, including CO_2-CH_4 interactions (part 1) and CO_2-H_2O wettability (part 2),[48] are vital for both CO_2 sequestration and methane recovery. This study (part 1) probes the real-time dynamic interactions between methane and CO_2 over multiple cycles of CO_2-ECBM injection using NMR technology. In the companion to this paper,[48] we investigate the dynamic interactions between CO_2 and H_2O over CO_2-ECBM flooding as a function of the injection pressure, temperature, and water occurrence state. The results are vital to better understand and evaluate controls of CO_2-ECBM improvement in recovery for enhanced gas recovery (EGR) and CO_2 geological sequestration.

2. COAL SAMPLES AND EXPERIMENTAL METHODS

2.1. Sampling. In this study, coal samples were collected from the southern Junggar Basin (sub-bituminous coal) and southern Qinshui Basin (anthracite), representing two of the most successful developed CBM reservoirs in China. The samples comprise deep-well cores (Figure 1) that were quickly packed and transported to the laboratory for a series of experiments. Basic petrophysical characteristics of the selected coal samples were measured, including maximum vitrinite reflectance ($R_{o,m}$) and maceral composition analysis, performed on the polished slabs using a Laborlux 12 POL microscope, following the China National Standards GB/T 6948-1998. Those data, together with core depth and *in situ* reservoir pressure, are presented in Table

https://dx.doi.org/10.1021/acs.energyfuels.0c01371
Energy Fuels 2020, 34, 8274−8282

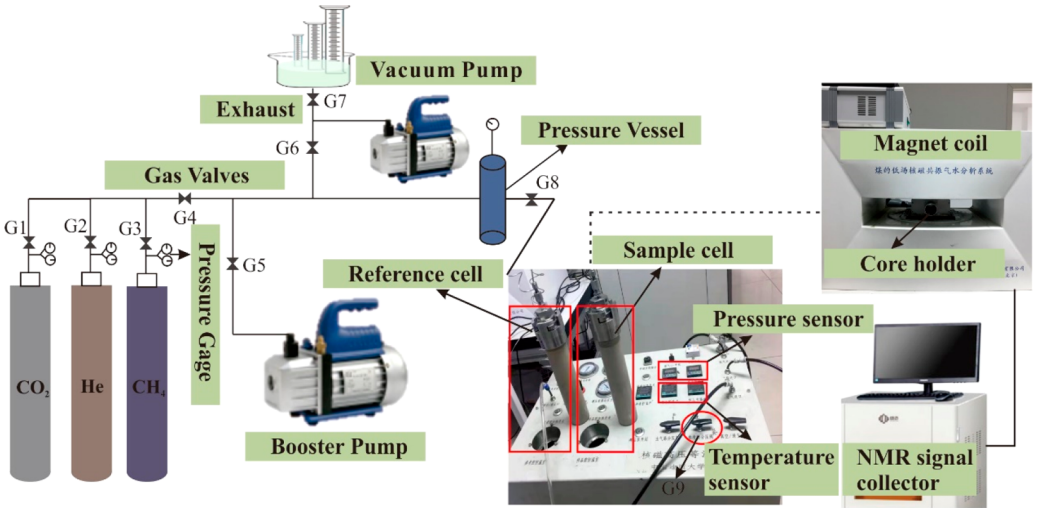

Figure 3. Schematic diagram of the NMR CO_2-ECBM experimental setup.

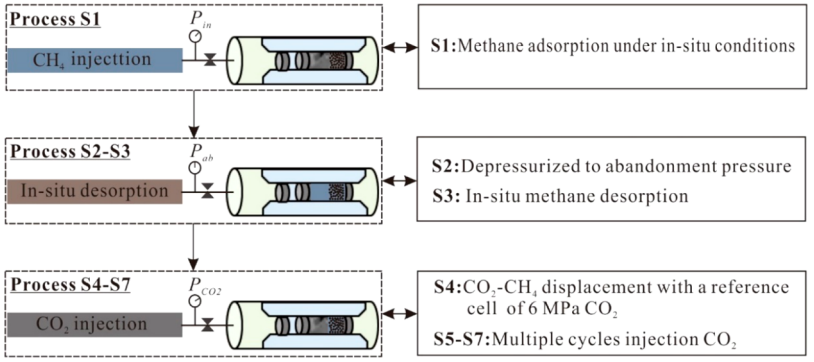

Figure 4. Schematic diagram of the experimental procedure.

1. The abandonment pressures (P_{ab}) for the two coals are 1.1 MPa for the sub-bituminous coal and 0.9 MPa for the anthracite.

Additionally, the CO_2 and methane adsorption isotherms for the selected two coal samples were determined by volumetric methods (Figure 2), followed by the experimental procedures used in previous studies.[45,46] Samples were prepared as powders with a particle size of 60−80 mesh, and the experimental temperature was ~303 K. For the sub-bituminous coal, the values of Langmuir volume for CO_2 and methane are 30.80 and 9.90 cm^3/g, respectively (Figure 2a). The anthracite has a CO_2 adsorption capacity of 32.87 cm^3/g and a methane adsorption capacity of 22.30 cm^3/g (Figure 2b). The Langmuir volume is much larger than that of methane for the selected coals, indicating preferential adsorption of CO_2 relative to methane.

2.2. Experimental Setup. NMR directly characterizes the hydrogen nuclei (^1H) present in reservoir fluids (i.e., methane and water) via the transverse relaxation time (T_2) distribution as[49,50]

$$\frac{1}{T_2} = \frac{1}{T_{2B}} + \frac{1}{T_{2S}} + \frac{1}{T_{2D}} \quad (1)$$

where T_{2B} is the bulk relaxation time, T_{2S} is the surface relaxation time, and T_{2D} is the diffuse relaxation time. With the application of a low-intensity homogeneous magnetic field and the assumption of the Carr−Purcell−Meiboom−Gill (CPMG) sequence, the parameters T_{2B} and T_{2D} in eq 1 can be ignored. Thus, eq 1 can be simply expressed as

$$\frac{1}{T_2} = \frac{1}{T_{2S}} = F_S\left(\frac{\rho_2}{r}\right) \quad (2)$$

where ρ_2 is the surface relaxivity (μm/s), F_S is pore shape factor, and r is the pore size (μm). As seen in eq 2, T_2 can be served as an indicator for the location of ^1H; a longer T_2 indicates that the hydrogen nuclei are located in a larger size pore.

Figure 3 shows the NMR CO_2-ECBM experimental setup assembled and used for this study. It comprises a gas supply system, a gas exhaust system, a reference cell, a sample cell, and an NMR measurement device. The gas supply system comprises three different cylinder gases (He, CO_2, and CH_4) and a booster pump. He was used to measure the system of airtightness. CH_4 and CO_2 are used for the ECBM experiments to characterize methane adsorption and the CO_2−CH_4 displacement capacity of coals. The gas exhaust system contains a vacuum pump and an exhaust collector, for waste gas recovery. The sample cell encloses the samples during the experiments, fabricated from non-magnetic polyether ether ketone (PEEK). Additionally, the sample cell is also designed to control both the temperature and pressure by the temperature sensor and pressure sensor, respectively. The reference cell accommodates and sustains the methane pressure under identical pressure to the sample cell. In this study, the NMR measurement parameter were set as 0.3 ms echo spacing, 6000 ms waiting time, and 10 000 echo numbers.

2.3. Experimental Procedures. Prior to the CO_2-ECBM experiments, the sample cell is purged by He gas to remove any contamination by impurities. For experimental sample preparation, the coal was powdered to 60−80 mesh (size of 0.18−0.25 mm) and then dried under 374.15 K for 12 h in an oven to remove any internal moisture. A series of seven continuous experiments (as shown in Figure 4) were designed to simulate multiple cycle injection of CO_2-ECBM behavior replicating *in situ* desorption.

2.3.1. S1 (Methane Adsorption under In Situ Conditions). The coal samples were placed in the sample cell, and a vacuum was applied for 3 h. Methane was injected into the reference cell at 6 MPa, and valve G9 was opened (Figure 3) to fill the sample cell with methane to

https://dx.doi.org/10.1021/acs.energyfuels.0c01371
Energy Fuels 2020, 34, 8274−8282

a pressure of P_{in} (*in situ* reservoir pressure, as listed in Table 1). The T_2 relaxation of the sample cell was then measured with an interval time of 60 min.

2.3.2. S2 and S3 (Methane Desorption under In Situ Conditions). Following process S1, the sample cell was depressurized to P_{ab} (abandonment pressure, as listed in Table 1) with the T_2 spectrum measured immediately (process S2). This procedure was then repeated until the difference between two successive measurements was virtually invariant (process S3).

2.3.3. S4–S7 (CO_2–CH_4 Displacement under Multiple Cycles of CO_2 Injection). (a) CO_2 was injected at 6 MPa into the reference cell, and then the gas valve G9 was opened to fill the sample cell from the reference cell (Figure 3). (b) The sample cell T_2 spectrum was measured every 60 min until the change between subsequent T_2 amplitudes was negligible. (c) The sample cell CO_2 pressure was increased, and experimental producers in step b were repeated at four incremented pressures for S5–S7.

3. RESULTS AND DISCUSSION

3.1. Quantitative NMR Model for Free and Adsorbed Methane. Defining a model for the quantitative characterization of free methane based on the NMR data alone is an indispensable requirement in characterizing the CO_2-ECBM rejection efficiency of methane. Figure 5 shows that NMR T_2 distributions at different pressures of free methane with these spectra exhibit a clear peak supplement by a long relaxation time of ~60–2000 ms. The T_2 spectra systematically shift to the right with increasing methane pressure, consistent with prior observation.[45] As shown in Figure 6a, the NMR free methane spectra amplitude is linearly related to bulk methane mass, as

$$M_{fre} = 0.000015A_{fre} \quad (3)$$

where M_{fre} is free methane mass (mol) and A_{fre} is the free methane amplitude of measured NMR T_2 relaxation.

It should be noted that the adsorbed methane mass cannot be calculated directly from eq 3. Different relaxation mechanisms contribute to the various occurrences of methane (adsorbed methane dominated by surface relaxation and free methane related to bulk relaxation) and may induce a significant error in the estimation of adsorbed methane mass. Thus, a calibration model must be developed for adsorbed methane; more details about adsorbed methane NMR quantification can be found in the studies of Wang et al.,[46] Liu et al.,[47] and Yao et al.[51] In this study, as shown in Figure 6b, an excellent linear correlation between the adsorbed methane T_2 amplitude and adsorbed methane mass results.

$$M_{ads} = 0.00001A_{ads} \quad (4)$$

where M_{ads} is the adsorbed methane mass (mol) and A_{ads} is the adsorbed methane NMR T_2 amplitude.

3.2. Methane Adsorption NMR T_2 Distributions. The results of the methane adsorption T_2 spectra at different pressures for the two selected coals are shown in Figure 7. The methane adsorption T_2 spectra exhibit three peaks: P1 (T_2 = 0.1–8 ms), P2 (T_2 = 20–300 ms), and P3 (T_2 = 300–2000 ms). It should be noted that the T_2 amplitude of the dry samples (black hollow squares in Figure 7) is extremely small compared to the methane adsorption T_2 spectra, indicating that the NMR signal from the coal matrix can be neglected. Therefore, the NMR spectra in Figure 7 solely represent the T_2 relaxation characteristics of methane. On the basis of the measurement principle of NMR embodied in eq 2 and prior results,[45] the multiphase nature of methane in coals may be classified into three parts: (a) adsorbed methane in coal micropores or on the matrix surface corresponding to the P1 peak, (b) non-adsorbed/free methane in coal mesopores/fractures represented by the P2 peak, and (c) non-adsorbed methane in coal particles or free space within the sample cell, corresponding to the P3 peak. To simplify the study, we used these metrics to classify methane in coals into adsorbed and non-adsorbed methane components.

The known solid mass of the powdered sample and the measured adsorbed mass of methane (calculated by eq 4) that

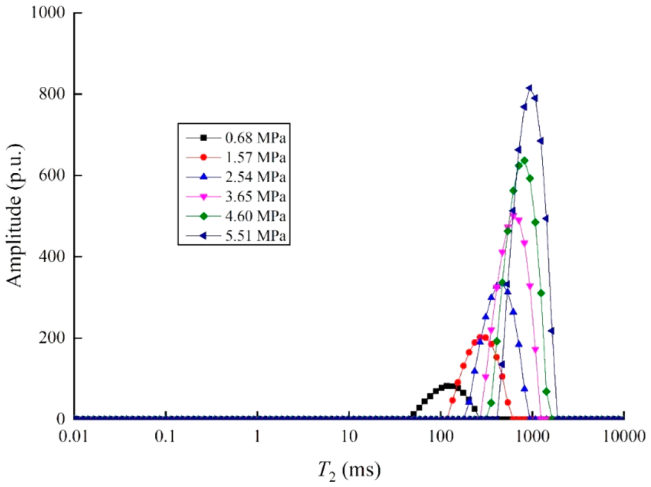

Figure 5. NMR T_2 distributions of free methane at different pressures.

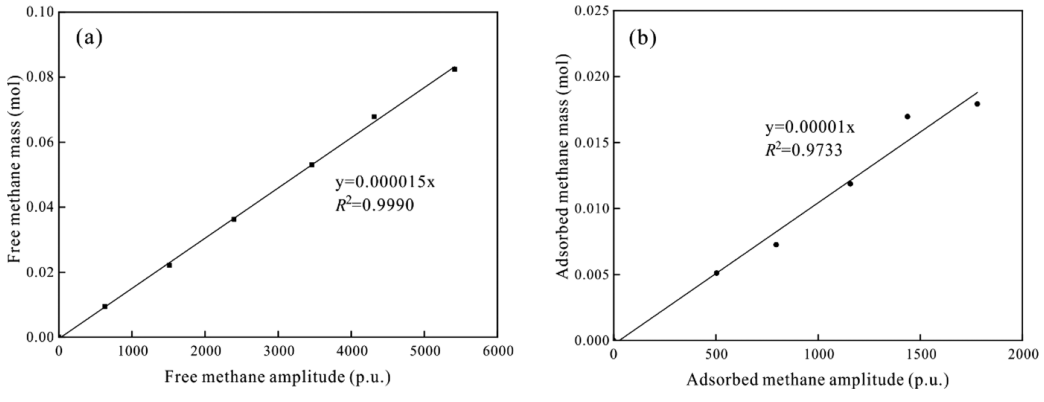

Figure 6. Relationship between the NMR T_2 amplitude relative to (a) free methane mass and (b) adsorbed methane mass.

https://dx.doi.org/10.1021/acs.energyfuels.0c01371
Energy Fuels 2020, 34, 8274–8282

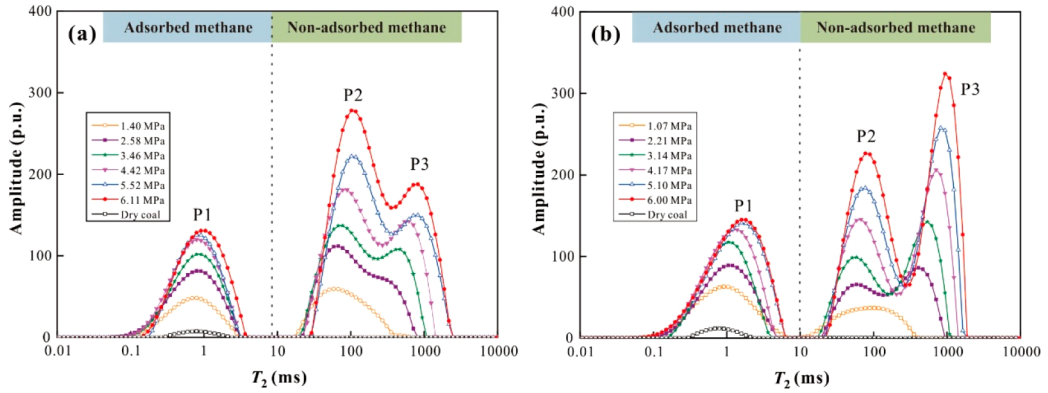

Figure 7. T_2 relaxation characteristics of methane adsorption under different pressures for the selected coal samples (a, sub-bituminous coal; b, anthracite).

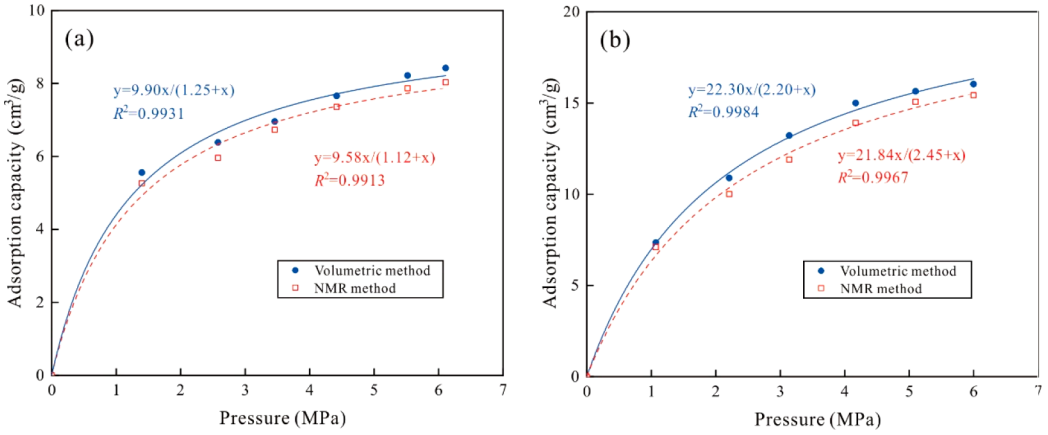

Figure 8. Comparison of adsorption isotherms determined by both the volumetric method and NMR (a, sub-bituminous coal; b, anthracite).

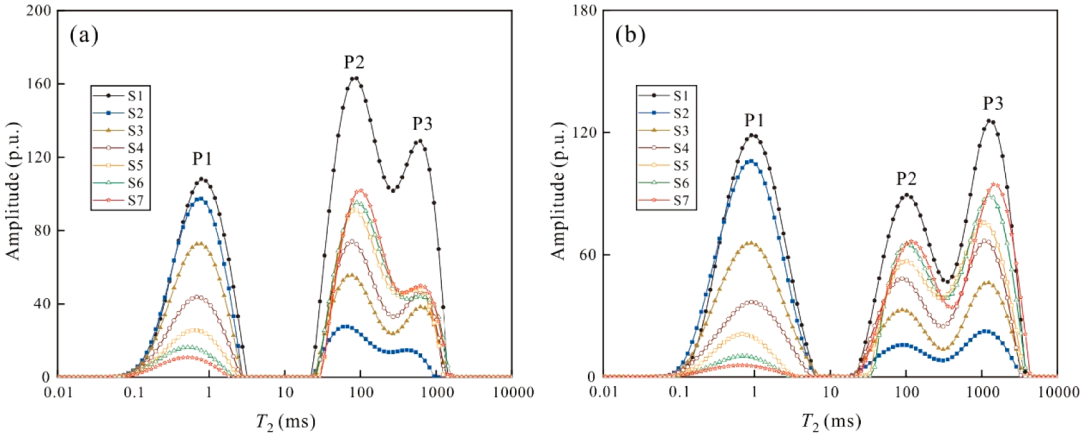

Figure 9. T_2 relaxation characteristics of methane during the processes S1−S7 (a, sub-bituminous coal; b, anthracite).

allow for methane adsorption capacity to be defined for the experimental pressures were plotted as red hollow squares in Figure 8. The NMR adsorption data fit well to the Langmuir relation (red dotted line in Figure 8), with correlation coefficients of >0.99 for both coals. Additionally, the adsorption isotherms evaluated by NMR show excellent agreement with those recovered from the volumetric method. The comparative results from NMR and volumetric methods demonstrate that the relative deviations from the Langmuir volume fall within <4.0%, an allowable error. It should be noted that the Langmuir volume determined from the NMR method is a little smaller than that from the volumetric method, possibly because the echo spacing of the NMR instrument used in this study defaulted as 0.3 ms, which cannot well-detect adsorbed methane with T_2 < 0.1 ms. These results suggest that the NMR measurement represents a high-efficiency tool for the quantitative characterization of adsorbed methane capacity in coals. In other words, it is feasible to investigate CO_2-ECBM response and effectiveness from the prospective of de/adsorbed methane based solely on the NMR relaxation measurement alone.

https://dx.doi.org/10.1021/acs.energyfuels.0c01371
Energy Fuels 2020, 34, 8274−8282

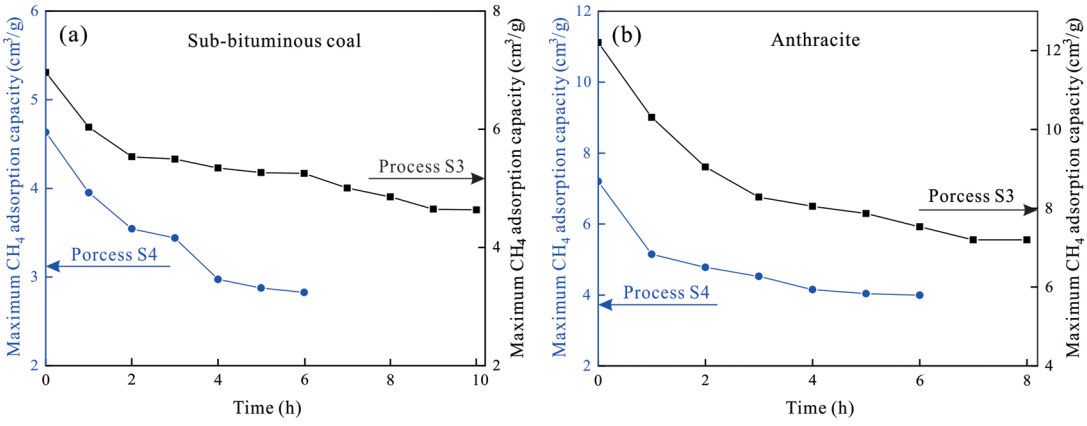

Figure 10. Real-time changes in maximum methane adsorption capacity during processes S3 and S4.

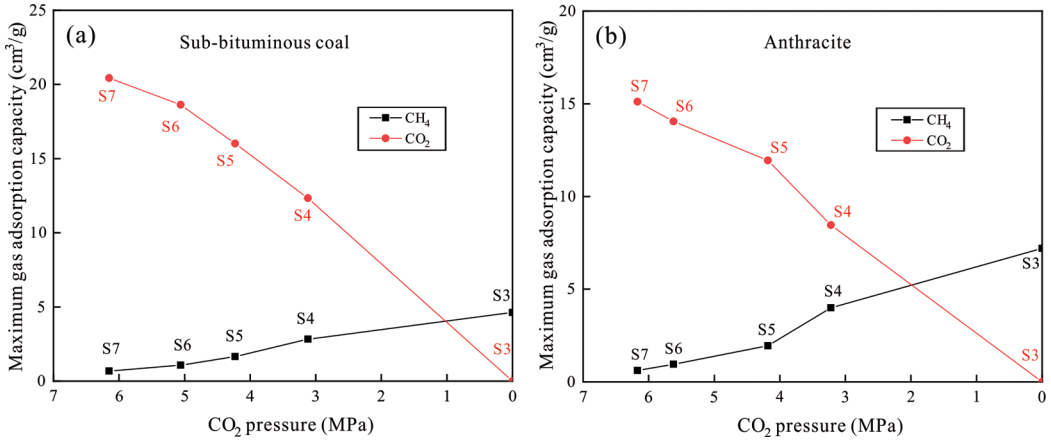

Figure 11. CO_2 and methane adsorption capacities in processes S3−S7.

3.3. Characterization of CO_2-ECBM under *In Situ* Conditions. Reservoir depressurization is the most commonly used method for CBM recovery.[6−9] However, it is difficult to achieve full CBM recovery using this method alone as a result of the high methane adsorption affinity for coals. In this section, we first evaluate the NMR methane T_2 distributions over multiple cycles of CO_2 injection (processes S4−S7) following *in situ* desorption (processes S2 and S3) by depressurization alone. Then, we discuss the implication of multiple cycles of CO_2 injection for EGR in sub-bituminous coal and anthracite. Finally, the implications of CO_2-ECBM for CO_2 geological sequestration and storage in coals are investigated. We use changes in the amplitudes of the T_2 peaks as proxies for gas mass concentrations in various reservoirs and various states, both adsorbed and as free gas.

3.3.1. Methane T_2 Distributions after Multiple Cycles of CO_2 Injection. Figure 9 shows the NMR T_2 distributions for the CO_2-ECBM displacement under *in situ* conditions. The amplitude of the adsorbed methane (i.e., P1) and non-adsorbed methane (i.e., P2 and P3) T_2 peaks decreases with depressurization to abandonment pressure (processes S1 and S2). This quantifies the desorption of adsorbed methane and its recovery of free methane. At the conclusion of the *in situ* desorption (processes S2 and S3), the adsorbed methane T_2 amplitude has decreased and the non-adsorbed methane amplitude significantly increased, suggesting exchange from the adsorbed state to free gas.

Following the first injection of CO_2 (process S4), adsorbed methane is released from storage but some residual adsorbed methane remains (Figure 9). With the following repeated cycles of CO_2 injection (processes S5−S7), the mass of adsorbed methane further decreases and is stored in the sample as free gas (Figure 9), identifying the utility of multiple cycles of CO_2-ECBM as an effective method of EGR.

3.3.2. Dynamic Changes in Methane Storage with and without CO_2 Injection. The most important use of the NMR method is to non-invasively monitor real-time dynamic changes in ^1H mass within the reservoir fluids (water or methane). Reduction in the amplitude of the P1 peaks represents the reduction in adsorbed methane mass, with the P2 and P3 peaks corresponding to masses of non-adsorbed methane in either the macropores/fractures and sample headspace, respectively. We use these proxies to investigate dynamic changes in CO_2−CH_4 displacement.

Figure 10 displays the real-time dynamic changes in maximum methane adsorption capacity resulting from both depressurization to abandonment pressure (process S3) by the first injection of CO_2 (process S4). During depressurization, the sub-bituminous coal fully desorbs over 10 h, with the maximum methane adsorption capacity falling from 6.96 to 4.63 cm^3/g. For anthracite, the maximum methane adsorption capacity decreases both larger and faster, falling from 12.20 to 7.20 cm^3/g over only 8 h. During this initial depressurization, the real-time variation in maximum methane adsorption

https://dx.doi.org/10.1021/acs.energyfuels.0c01371
Energy Fuels 2020, 34, 8274−8282

capacity occurs in two stages: a rapid initial decline followed by a slower tail.

The maximum methane adsorption capacity further decreases with the first injection of CO_2 (process S4) (Figure 10); preferential adsorption of CO_2 rejects methane as a free gas. Again, two different CO_2−CH_4 displacement rates are apparent: an initial rapid competitive desorption of methane followed by a long desorption tail (Figure 10). For the sub-bituminous coal, the methane content declines rapidly in the first 2 h, while for the anthracite, this rapid decline endures for only 1 h (Figure 10).

3.3.3. Implications for Enhanced Methane Recovery in Coals. Coal has a higher adsorption capacity of CO_2 relative to methane, making EGR feasible. The benefit of applying repeated injections of CO_2 is shown in Figure 11a. The maximum methane adsorption content of sub-bituminous coal decreases from 4.63 to 0.69 cm^3/g over the following four cycles (S3 and then S4−S7), indicating a cumulative yield of 3.94 cm^3/g of adsorbed methane desorbed by CO_2. For the anthracite, the adsorbed methane content falls from 7.20 to 0.61 cm^3/g (S3 and then S4−S7), suggesting that 91.5% of adsorbed methane is displaced over the multiple cycles of CO_2 injections following *in situ* desorption (Figure 11b).

To quantitatively characterize the effectiveness of EGR, both with and without multiple cycles of CO_2 injection, methane sweep efficiency (ω) is defined as

$$\omega_{Si} = \frac{Q_{Si}}{Q_f} \times 100\% \tag{5}$$

where ω_{Si} is the methane sweep efficiency following the experimental process Si (i = 3, 4, 5, 6, and 7) (%), Q_{Si} represents the volume per unit coal mass of adsorbed methane following process Si (cm^3/g), and Q_f represents the volume per unit coal mass of adsorbed methane when fully saturated at pressure P_{in} (cm^3/g).

Methane sweep efficiency following initial depressurization (−S3) followed by repeated CO_2 injection (S4−S7) is shown in Figure 12. For the sub-bituminous coal, only 43.42% of adsorbed methane is desorbed after *in situ* desorption (process S3), with a large significant mass of methane remaining adsorbed to the coal matrix. With the first injection of CO_2 (process S4), the methane sweep efficiency increases to 59.50%, indicating that more than 16% of adsorbed methane is displaced and desorbed by CO_2 (Figure 12a). However, more than 40% of methane remains within the coal matrix surface following the first injection of CO_2, suggesting the need for multiple cycled injections of CO_2. Repeated multiple injection cycles of CO_2 increase the desorption efficiency to 82.15% at the end of injection S7 (Figure 12a). Thus, ∼22.75% of adsorbed methane is transformed into free gas over four cycles of CO_2 injection, relative to a single cycle.

For the anthracite, the methane sweep efficiency increases from 67.29 to 95.01% over the same four cycles of injection (processes S4−S7), liberating ∼28% of adsorbed methane as a result of the multiple cycles of CO_2 injection (Figure 12b). Thus, for both sub-bituminous coal and anthracite, the application of multiple cycles of CO_2 injection is advantageous.

The sub-bituminous coal and anthracite are from the southern Junggar Basin and southern Qinshui Basin, respectively. After more than 10 years of development, methane recovery in the Qinshui Basin anthracites has already begun to decrease. Conversely, development in the southern

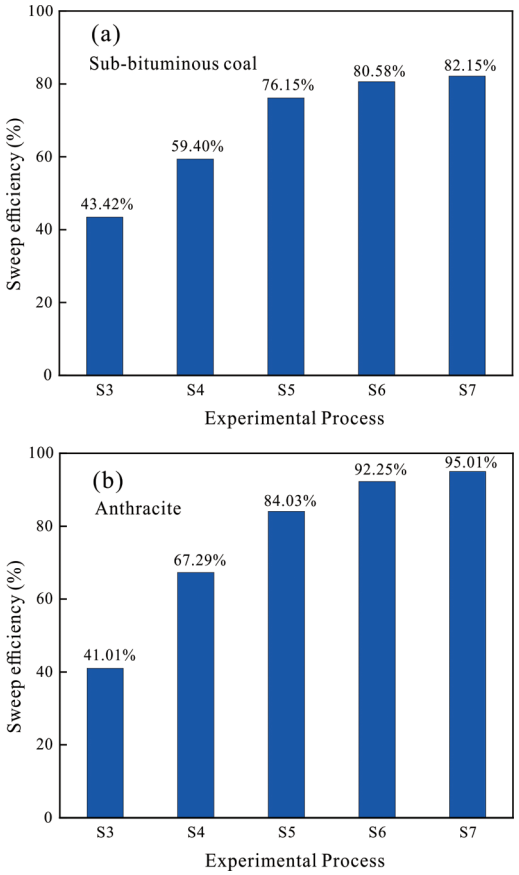

Figure 12. Methane sweep efficiency in processes S3−S7 for the coals.

Junggar Basin is relatively recent, with CBM production of the sub-bituminous coals continuing at sub-optimal rates.[52] The results of CO_2-ECBM EGR suggest that the multiple cycles of CO_2 injection could significantly improve the methane sweep efficiency and corresponding methane recovery from these coals.

3.3.4. Implications for CO_2 Geological Sequestration and Storage in Coals. In addition to enhancing methane recovery, injecting CO_2 into coal reservoirs also provides CO_2 geological sequestration and storage. Injected CO_2 will exist as an adsorbed phase within the coal matrix surface and also as a free phase in fractures and dissolved within the interstitial water. The mass of CO_2 present within the dissolved phase is typically negligible relative to the adsorbed phase content. We estimate the CO_2 sequestration capacity of coals as an adsorbed phase. The mass of adsorbed CO_2 resulting from CO_2-ECBM can be calculated from[20]

$$M_{ads\text{-}CO_2} = \frac{P_r V_r}{Z_r RT} - \frac{P_e V_{fre}}{Z_e RT} - M_{ads\text{-}CH_4} \tag{6}$$

where $M_{ads\text{-}CO_2}$ and $M_{ads\text{-}CH_4}$ are the masses of adsorbed CO_2 and methane, respectively (cm^3/g), P_r is the CO_2 injection pressure at a reference (cell) pressure (MPa), P_e is the equilibrated pressure in the sample cell (MPa), Z_b and Z_e are the compression factors at P_r and P_e, respectively, R is the gas content (8.3144 J mol^{-1} K^{-1}), and T is the experimental temperature (K).

On the basis of eq 6, maximum adsorbed CO_2 resulting from injections S4−S7 is calculated and shown as red dots in Figure

https://dx.doi.org/10.1021/acs.energyfuels.0c01371
Energy Fuels 2020, 34, 8274−8282

11. The maximum CO_2 adsorption capacity increases with an increase in the pressure of the sample cell, with a corresponding reduction in methane adsorption capacity. For the sub-bituminous coal, the maximum adsorbed CO_2 content is 12.34 cm^3/g after a single injection of CO_2 (process S4) that increases to 20.43 cm^3/g at the equilibrium pressure of the sample cell at 6.15 MPa (process S7). For the anthracite, the maximum CO_2 adsorption capacity increases from 8.56 to 15.11 cm^3/g over the multiple cycles of CO_2 injection, suggesting that a total of 6.55 cm^3/g CO_2 is absorbed into the coal matrix and correspondingly sequestered.

Figure 13 shows the relationship between the maximum methane adsorption capacity and maximum CO_2 adsorption

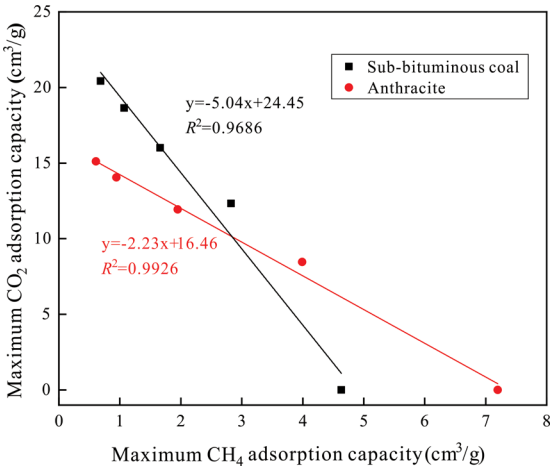

Figure 13. Relationship between the maximum methane adsorption capacity and maximum CO_2 adsorption capacity in processes S3−S7 for the sub-bituminous coal and anthracite.

capacity during both depressurization (process S3) and multiple cycles of CO_2 injection (processes S4−S7). A flat gradient represents a desired response for enhanced methane desorption (with a small injected mass of CO_2) in anthracite, and a steep gradient represents desirable characteristics as a CO_2 sequestration target for sub-bituminous coal (small amount of methane desorbed with a large mass of CO_2 stored). On the basis of the assumption of a desired residual adsorbed methane content approaching 0 cm^3/g, the maximum sequestered CO_2 content can be estimated from the correlated equations in Figure 13; these are 24.45 and 16.46 cm^3/g, corresponding to sub-bituminous coal and anthracite, respectively. Although methane sweep efficiency cannot reach 100% in reality, multiple cycles of CO_2 injection allow for this ideal state to be approached.

As shown in Figures 12 and 13, during the process of CO_2-ECBM, the sub-bituminous coal has a higher CO_2 geological sequestration content than that of anthracite. Whereas the methane recovery of anthracite was much larger relative to sub-bituminous coal over multiple cycles of injection of CO_2. These results indicate that multiple cycles of CO_2 injection applied in southern Junggar Basin sub-bituminous coals are more effective for CO_2 sequestration and storage, while southern Qinshui Basin anthracite benefits more in terms of enhanced methane production, per unit mass of CO_2 injection.

4. CONCLUSION

We evaluate real-time dynamic changes of adsorbed/non-adsorbed methane during multiple cycles of CO_2-ECBM flooding under *in situ* conditions using calibrated NMR. The main conclusions are summarized as follows: (1) The T_2 distribution of methane exhibits three peaks in coals: P1 (T_2 = 0.1−8 ms), P2 (T_2 = 20−300 ms), and P3 (T_2 = 300−2000 ms), corresponding to adsorbed methane in the coal matrix, non-adsorbed methane within the pores, and finally within the headspace of the sample cell, respectively. The adsorption isotherms quantitatively evaluated from the NMR show excellent agreement with those from volumetric parallel measurements that are used to calibrate the NMR method, with a relative Langmuir volume deviation of <4.0%. (2) CO_2−CH_4 flooding experiments exhibit two distinct ad/desorption rates: the first represents a rapid decline in the methane content that stabilizes following a long desorptive tail. In comparison to the conventional reservoir depressurization, multiple cycles of CO_2 injection improve methane recovery by ∼39% for sub-bituminous coal and ∼54% for anthracite, suggesting the utility of this novel flooding technology for enhancing methane recovery from coals. (3) The ratios of maximum CO_2 adsorption capacity relative to the corresponding CH_4 desorption capacity are nearly constant over multiple cycles of CO_2 injection. The observed values for this ratio are 5.0 and 2.2 for sub-bituminous coal and anthracite, respectively, and representing the elevated potential of sub-bituminous coals as a CO_2 sequestration medium and the desirable response of anthracite for CO_2-ECBM.

AUTHOR INFORMATION

Corresponding Author

Yanbin Yao − *School of Energy Resources and Coal Reservoir Laboratory of National Engineering Research Center of CBM Development & Utilization, China University of Geosciences, Beijing 100083, People's Republic of China;* orcid.org/0000-0003-3838-4305; Email: yyb@cugb.edu.cn

Authors

Sijian Zheng − *School of Energy Resources, Coal Reservoir Laboratory of National Engineering Research Center of CBM Development & Utilization, and Beijing Key Laboratory of Unconventional Natural Gas Geological Evaluation and Development Engineering, China University of Geosciences, Beijing 100083, People's Republic of China*

Derek Elsworth − *Department of Energy and Mineral Engineering, Pennsylvania State University, University Park, Pennsylvania 16802, United States*

Dameng Liu − *School of Energy Resources and Coal Reservoir Laboratory of National Engineering Research Center of CBM Development & Utilization, China University of Geosciences, Beijing 100083, People's Republic of China;* orcid.org/0000-0002-4688-074X

Yidong Cai − *School of Energy Resources and Coal Reservoir Laboratory of National Engineering Research Center of CBM Development & Utilization, China University of Geosciences, Beijing 100083, People's Republic of China;* orcid.org/0000-0002-4915-5615

Complete contact information is available at: https://pubs.acs.org/10.1021/acs.energyfuels.0c01371

https://dx.doi.org/10.1021/acs.energyfuels.0c01371
Energy Fuels 2020, 34, 8274−8282

Notes

The authors declare no competing financial interest.

■ ACKNOWLEDGMENTS

The authors acknowledge financial support from the National Natural Science Foundation of China (41830427 and 41872123), the National Major Science and Technology Projects of China (2016ZX05043-001), the Key Research and Development Project of Xinjiang Uygur Autonomous Region (2017B03019-1), the Foreign Cultural and Educational Experts Employment Program from Foreign Experts Service Division, Ministry of Science and Technology of People's Republic of China, and the Fundamental Research Funds for the Central Universities (292019252).

■ REFERENCES

(1) Sarkodie, S. A.; Strezov, V. *Sci. Total Environ.* **2019**, *646*, 862−871.
(2) Yan, H.; Zhang, J. X.; Zhou, N.; Li, M. *J. Nat. Gas Sci. Eng.* **2019**, *65*, 275−283.
(3) Meng, M.; Qiu, Z. S.; Zhong, R. Z.; Liu, Z. G.; Liu, Y. F.; Chen, P. *Chem. Eng. J.* **2019**, *368*, 847−864.
(4) Faiz, M. M.; Saghafi, A.; Barclay, S. A.; Stalker, L.; Sherwood, N. R.; Whitford, D. J. *Int. J. Greenhouse Gas Control* **2007**, *1*, 223−235.
(5) Qi, Y.; Ju, Y.; Cai, J.; Gao, Y.; Zhu, H.; Hunag, C.; Wu, J.; Meng, S.; Chen, W. *Fuel* **2019**, *235*, 72−84.
(6) Liu, J.; Xie, L. Z.; Elsworth, D.; Gan, Q. *Environ. Sci. Technol.* **2019**, *53*, 9328−9336.
(7) Cao, T. Y.; Huang, K.; Shi, Y. X.; Cai, N. S. *Energy Environ. Sci.* **2017**, *10*, 460−490.
(8) Karacan, C. Ö.; Ruiz, F. A.; Cotè, M.; Phipps, S. *Int. J. Coal Geol.* **2011**, *86*, 121−156.
(9) Moore, T. A. *Int. J. Coal Geol.* **2012**, *101*, 36−81.
(10) Yu, K.; Ju, Y. W.; Qian, J.; Qu, Z. H.; Shao, C. J.; Yu, K. L.; Shi, Y. *Int. J. Coal Geol.* **2018**, *198*, 100−115.
(11) Li, Q. G.; Ju, Y. W.; Bao, Y.; Yan, Z. F.; Li, X. S.; Sun, Y. *Energy Fuels* **2015**, *29* (2), 546−555.
(12) Cai, Y. D.; Liu, D. M.; Mathews, J. P.; Pan, Z. J.; Elsworth, D.; Yao, Y. B.; Li, J. Q.; Guo, X. Q. *Int. J. Coal Geol.* **2014**, *122*, 91−104.
(13) Zheng, S. J.; Yao, Y. B.; Liu, D. M.; Cai, Y. D.; Liu, Y. *Int. J. Coal Geol.* **2019**, *205*, 1−13.
(14) Ranathunga, A. S.; Perera, M. S. A.; Ranjith, P. G.; Wei, C. G. *Fuel* **2017**, *189*, 391−399.
(15) Zhang, X. G.; Ranjith, P. G. *J. CO2 Util.* **2019**, *33*, 394−404.
(16) Pan, Z. J.; Connell, L. D.; Camilleri, M. *Int. J. Coal Geol.* **2010**, *82*, 252−261.
(17) Liu, Z. D.; Cheng, Y. P.; Wang, Y. K.; Wang, L.; Li, W. *Fuel* **2019**, *236*, 709−716.
(18) Meng, M.; Qiu, Z. S. *Fuel* **2018**, *219*, 223−238.
(19) Guan, C.; Liu, S. M.; Li, C. W.; Wang, Y.; Zhao, Y. X. *Fuel* **2018**, *211*, 241−250.
(20) Dutka, B. *Fuel* **2019**, *247*, 228−236.
(21) Clarkson, C. *SPE J.* **2003**, *8* (03), 236−251.
(22) Connell, L. D.; Pan, Z. J.; Camilleri, M. *Int. J. Coal Geol.* **2019**, *201*, 62−75.
(23) Pajdak, A.; Kudasik, M.; Skoczylas, N.; Wierzbicki, M.; Teixeira Palla Braga, L. *Int. J. Greenhouse Gas Control* **2019**, *90*, 102789.
(24) Harpalani, S.; Mitra, A. *Transp. Porous Media* **2010**, *82* (1), 141−156.
(25) Hou, H. H.; Shao, L. Y.; Li, Y. H.; Li, Z.; Wang, S.; Zhang, W. L.; Wang, X. T. *J. Pet. Sci. Eng.* **2017**, *149*, 218−227.
(26) Sun, Y. F.; Zhao, Y. X.; Yuan, L. *J. Nat. Gas Sci. Eng.* **2018**, *54*, 202−215.
(27) Liu, C. J.; Sang, S. X.; Zhang, K.; Song, F.; Wang, H. W.; Fan, X. F. *J. CO2 Util.* **2019**, *34*, 343−352.
(28) Reeves, S. R. *Carbon Dioxide Sequestration in Geological Media—State of the Science*, 2009. DOI: 10.1306/13171231St593373
(29) Pan, Z. J.; Ye, J. P.; Zhou, F. B.; Tan, Y. L.; Connell, L. D.; Fan, J. J. *Int. Geol. Rev.* **2018**, *60*, 754−776.
(30) Wong, S.; Law, D.; Deng, X.; Robinson, J.; Kadatz, B.; Gunter, W. D.; Jianping, Y.; Sanli, F.; Zhiqiang, F. *Int. J. Greenhouse Gas Control* **2007**, *1*, 215−222.
(31) Kedzior, S. *Int. J. Coal Geol.* **2009**, *80*, 20−34.
(32) Wang, Q. Q.; Li, W.; Zhang, D. F.; Wang, H. H.; Jiang, W. P.; Zhu, L.; Tao, J.; Huo, P. L.; Zhang, J. J. *J. Nat. Gas Sci. Eng.* **2016**, *34*, 811−822.
(33) Vishal, V.; Mahanta, B.; Pradhan, S. P.; Singh, T. N.; Ranjith, P. G. *Energy* **2018**, *159*, 1185−1194.
(34) Fulton, P. F.; Parente, C. A.; Rogers, B. A.; Shah, N.; Reznik, A. A. A Laboratory Investigation of Enhanced Recovery of Methane from Coal by Carbon Dioxide Injection. *Proceedings of the SPE Unconventional Gas Recovery Symposium*; Pittsburgh, PA, May 18−21, 1980; DOI: 10.2118/8930-MS.
(35) Dutka, B.; Kudasik, M.; Topolnicki, J. *Fuel Process. Technol.* **2012**, *100*, 30−34.
(36) Dutka, B.; Kudasik, M.; Pokryszka, Z.; Skoczylas, N.; Topolnicki, J.; Wierzbicki, M. *Fuel Process. Technol.* **2013**, *106*, 95−101.
(37) Xu, J. Z.; Zhai, C.; Liu, S. M.; Qin, L.; Wu, S. J. *Fuel* **2017**, *208*, 41−51.
(38) Edlmann, K.; Hinchliffe, S.; Heinemann, N.; Johnson, G.; Ennis-King, J.; Mcdermott, C. I. *Int. J. Greenhouse Gas Control* **2019**, *80*, 1−9.
(39) Timur, A. *JPT, J. Pet. Technol.* **1969**, *21*, 775−786.
(40) Yao, Y. B.; Liu, D. M.; Che, Y.; Tang, D. Z.; Tang, S. H.; Huang, W. H. *Fuel* **2010**, *89*, 1371−1380.
(41) Zhao, Y. X.; Zhu, G. P.; Dong, Y. H.; Danesh, N. N.; Chen, Z. W.; Zhang, T. *Fuel* **2017**, *210*, 217−226.
(42) Li, X.; Fu, X. H.; Ranjith, P. G.; Fang, Y. *J. Nat. Gas Sci. Eng.* **2018**, *57*, 189−202.
(43) Zheng, S. J.; Yao, Y. B.; Liu, D. M.; Cai, Y. D.; Liu, Y. *Int. J. Coal Geol.* **2018**, *196*, 148−158.
(44) Sun, X. X.; Yao, Y. B.; Liu, D. M.; Zhou, Y. *Int. J. Coal Geol.* **2018**, *188*, 38−50.
(45) Yao, Y. B.; Liu, D. M.; Xie, S. B. *Int. J. Coal Geol.* **2014**, *131*, 32−40.
(46) Wang, F.; Yao, Y. B.; Wen, Z. A.; Sun, Q. P.; Yuan, X. H. *Fuel* **2020**, *266*, 117102.
(47) Liu, J.; Yao, Y. B.; Liu, D. M.; Elsworth, D. *Int. J. Coal Geol.* **2017**, *179*, 211−218.
(48) Zheng, S. J.; Yao, Y. B.; Elsworth, D.; Liu, D. M.; Cai, Y. D. *Fuels* **2020**, DOI: 10.1016/j.fuel.2020.118560.
(49) Kleinberg, R. L.; Horsfield, M. A. *J. Magn. Reson.* **1990**, *88*, 9−19.
(50) Coates, G. R.; Xiao, L. Z.; Primmer, M. G. *NMR Logging Principles and Applications*; Gulf Publishing Company: Houston, TX, 1999.
(51) Yao, Y. B.; Liu, J.; Liu, D. M.; Chen, J. Y.; Pan, Z. J. *Int. J. Coal Geol.* **2019**, *201*, 76−85.
(52) Qin, Y.; Moore, T. A.; Shen, J.; Yang, Z. B.; Shen, Y. L.; Wang, G. *Int. Geol. Rev.* **2018**, *60*, 777−812.